

**Direct growth of highly branched single crystal Au nanostructures on  
electrode Surface: Their surface enhanced Raman scattering and  
electrocatalytic activity**

*HailanChen, KannanPalanisamy, CongWang, Hongyu Chen and*

*Dong-Hwan Kim\**

School of Chemical and Biomedical Engineering  
Nanyang Technological University  
70 Nanyang Drive, Singapore 637457

**Supporting information**

\*Corresponding author: Tel (65) 6790-4111; Fax (65) 6791-1761; e-mail:  
[dhkim@ntu.edu.sg](mailto:dhkim@ntu.edu.sg)

### **The effect of CTAB, HAuCl<sub>4</sub>, AA and SAM on BANCs growth**

To confirm the proposed mechanism, we have investigated the effect of concentrations of CTAB, HAuCl<sub>4</sub>, AA and HDT SAM on the morphology of BANCs. When a high concentration of CTAB (92 mM, this concentration is close to that for the synthesis of gold nanorod), the BANCs tend to be a single or twin nanocrystals (Figure S1, image a) and the number of branches per crystals increases as the concentration of CTAB decreases (Figure S1, image b-d). The effective BANCs growth occurs when 16 mM CTAB is used in the growth solution, indicating that 16 mM CTAB is a critical concentration for BANCs growth on the surface (Figure S1, image d). Finally, the length of branches and size of the BANCs were decreased at the lower conc. of CTAB (2 mM) as presented in Figure 5, image e. Further, we have studied the effect of concentration of HAuCl<sub>4</sub> for the growth of BANCs and the HAuCl<sub>4</sub> associated morphology changes (Figure S2). When the concentration of HAuCl<sub>4</sub> is doubled, high density of BANCs is grown (close distribution of BANCs) on the surface and significantly high concentration of HAuCl<sub>4</sub> (ten times higher) produces small clusters especially sphere-like Au nanoparticles with different sizes without branches (Figure S2, image a). The lower concentration of HAuCl<sub>4</sub> results in smaller BANCs with less number of branches (indistinguishable) and the corresponding SEM image is shown in Figure S2, image f. Thus, the concentration of HAuCl<sub>4</sub> (1 mM) is also crucial to control the size of particle, density and branches of the nanocrystals.

Then, the similar way, higher concentration of AA (40 mM) can produce single branch with uniform density of the nanocrystals (Figure S3, image a) and the lower concentration (0.2 mM) can produce more branched nanocrystals with few

indistinguishable branches (Figure S3, image f), when compared to higher concentration of AA (40 mM) as shown in Figure S3, image a. It is worth to discuss that of the higher concentration of AA leads to ill-defined growth of BANCs on the surface, while the lower concentration of AA produced smaller size of BANCs due to the insufficient amount of  $\text{Au}^0$  produced by AA. The branches of BANCs were increases notably (Figure S3, image d) at 4mM of AA and this conc. is highly optimum for the growth of BANCs on the surface. Finally, we have also investigated the effect of HDT SAM on the growth of BANCs. The BANCs were grown on wafers modified with series of concentrations of HDT as shown in Figure S4. In the absence of HDT SAM, BANCs still can grow on the wafers, and showed that highly dense and vertically assembled less branched nanostructures (Figure S4, image a). In the presence of 0.01 and 0.1 mM conc. of HDT SAM, the high density of gold nanoparticles with branched shape was formed (Figure S4, images b and c). After that, the substrate modified with higher concentration of HDT ( $\geq 15$  mM), more branched and larger amount of BANCs were formed (Figure S4, image e). It concludes that 15 mM of HDT was effective to produce high coverage of BANCs on the HDT SAM modified conducting surface.

### **Electrochemical characterization of surface grown BANCs**

Cyclic voltammetry (CV) of the reversible electroactive species  $[\text{Fe}(\text{CN})_6]^{3-/4-}$  is a convenient tool for testing the kinetics barrier of the interface. The CV responses of the bare Au, HDT, BANCs electrodes were examined by taking the  $[\text{Fe}(\text{CN})_6]^{3-/4-}$  redox couple in 0.1 M PBS as a model and the CVs were shown in Figure S5(a). The bare Au electrode shows a reversible voltammogram with a peak to peak separation ( $\Delta E_p$ ) of 110 mV for the  $[\text{Fe}(\text{CN})_6]^{3-/4-}$  couple characteristic of a diffusion-controlled redox process

(black line), whereas the HDT modified electrode showed a sluggish voltammetric response, with a  $\Delta E_p$  value of more than 300 mV, indicating that the HDT monolayer on the electrode surface hinders the electron-transfer kinetics (blue line). On the other hand, a significant increase in the peak current associated with a decrease in the  $\Delta E_p$  value (~82 mV) was noticed at BANCs electrode. The peak current and  $\Delta E_p$  value observed at the BANCs electrode are higher than the unmodified polycrystalline Au electrode, indicating that the BANCs on the HDT monolayer favor the electron-transfer reaction over the redox reaction and it is suggested that the nanoparticles function as an 'electron antenna', efficiently funneling electrons between the electrode and electrolyte. The electrochemical impedance measurements further support the favorable electron transfer kinetics on the BANCs electrode (Figure S5(b)). The  $|z|'$  value for BANCs modified electrode is 6.4 k $\Omega$  (red line), which is lower than the bare (7.6 k $\Omega$ ; black line) and HDT SAM modified electrodes (12.3 k $\Omega$ ; blue line). The increase in the active surface area with respect to the surface density of the BANCs on the electrode surface can play an important role in the electron transfer kinetics reaction (Figure S5(b)). Thus, the results extracted from EIS measurements connected with each step of the electrode modifications were in good agreement with the results obtained from CVs (Figure S5(a)). It has been shown that if electron tunneling across an insulating barrier is implicated in the electron-transfer process, the redox current at any potential should decrease exponentially with the barrier thickness according to the following expression<sup>1</sup>:

$$\mathbf{I} = \mathbf{I}_0 e^{-\beta d} \quad (1)$$

where  $I_0$  is the current measured at the bare electrode,  $\beta$  is the potential independent electron tunneling coefficient, and  $d$  is the thickness of the monolayer. For an electrochemical reaction at equilibrium, Eq. (2) can be obtained using Eq. (1):

$$k = k_0 e^{-\beta d} \quad (2)$$

where  $k_0$  and  $k$  are the electron-transfer rate constants at the bare Au and Au/HDT modified electrodes. Heterogeneous electron transfer rate constant ( $k_{et}$ ) at the bare and modified electrodes can be calculated using Eq. (3)<sup>2</sup>:

$$k_{et} = RT/n^2 F^2 A R_{CT} C_0 \quad (3)$$

where  $R$  is the gas constant,  $T$  is temperature (K),  $F$  is the Faraday constant,  $A$  is the electrode area ( $\text{cm}^2$ ),  $R_{CT}$  is the charge transfer resistance,  $C_0$  is the concentration of the redox couple in the bulk of solution ( $1 \times 10^{-3} \text{ mol/cm}^3$ ), and  $n$  is the number of transferred electrons per molecule of the redox probe ( $n$ ) one in the case of  $[\text{Fe}(\text{CN})_6]^{3-/4-}$  redox couple. The apparent charge transfer resistance values were obtained from fittings of the EIS spectra. The heterogeneous electron-transfer rate constant,  $k_{et}$ , estimated using Eq. (3) was found to be  $6.24 \times 10^{-6} \text{ cm.s}^{-1}$  for bare Au electrode,  $3.46 \times 10^{-7} \text{ cm.s}^{-1}$  for HDT SAM modified Au electrode and  $2.65 \times 10^{-6} \text{ cm.s}^{-1}$  for BANCs grown on the SAM HDT modified Au electrode. The highest  $k_{et}$  value obtained at surface grown BANCs electrode indicated that the fastest electron transfer kinetics takes place at the BANCs electrode.

## References

1. J. Xu, H.L. Li, Y. Zhang, *J. Phys. Chem.* 1993, **97**, 11497-11500.
2. M. Chirea, C.M. Pereira, F.A. Silva, *J. Phys. Chem. C* 2007, **111**, 9255-9266.

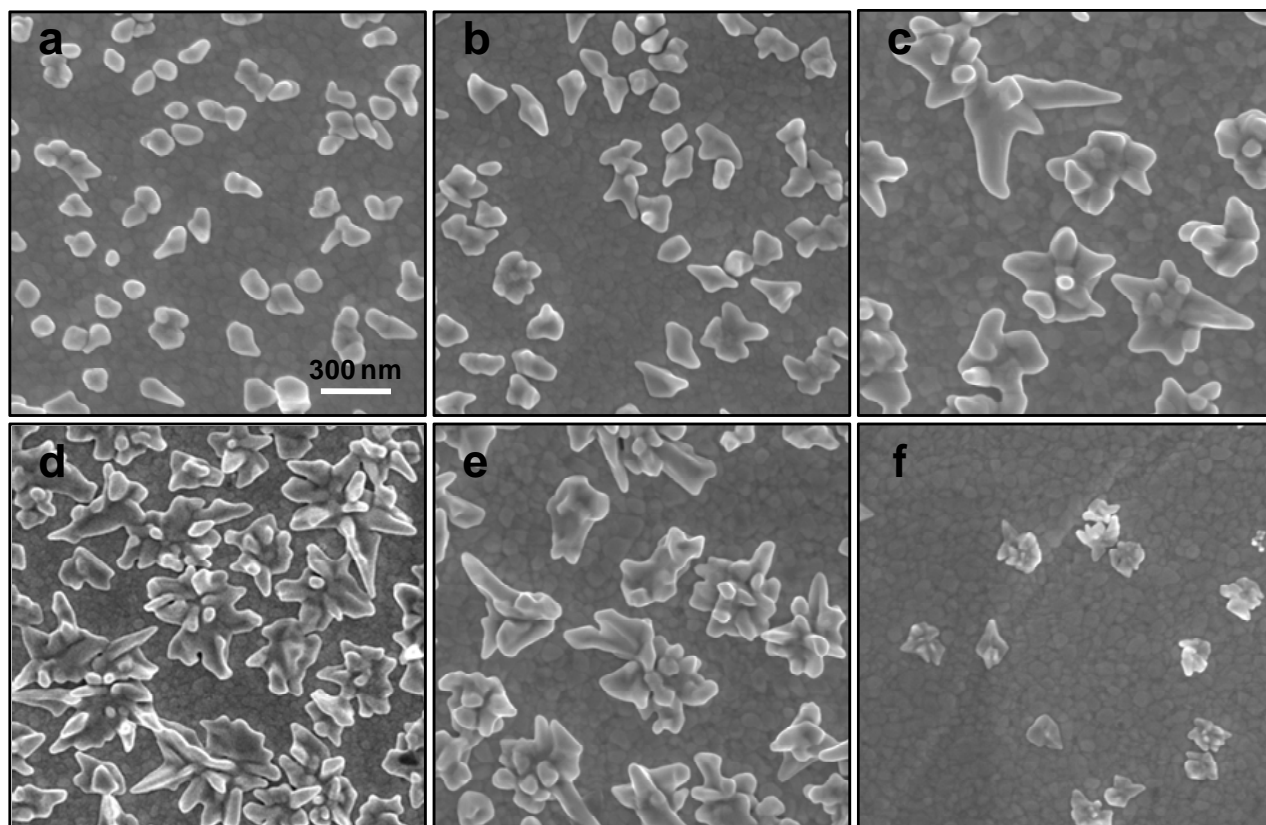


**Fig. S1** FESEM images (a-f) of BANCs (6 h growth) on Au-coated silicon wafer with respect to different conc. of CTAB (92, 48, 32, 16, 8, and 2mM). The conc. of  $\text{HAuCl}_4$  and AA is 1 mM and 4 mM respectively.

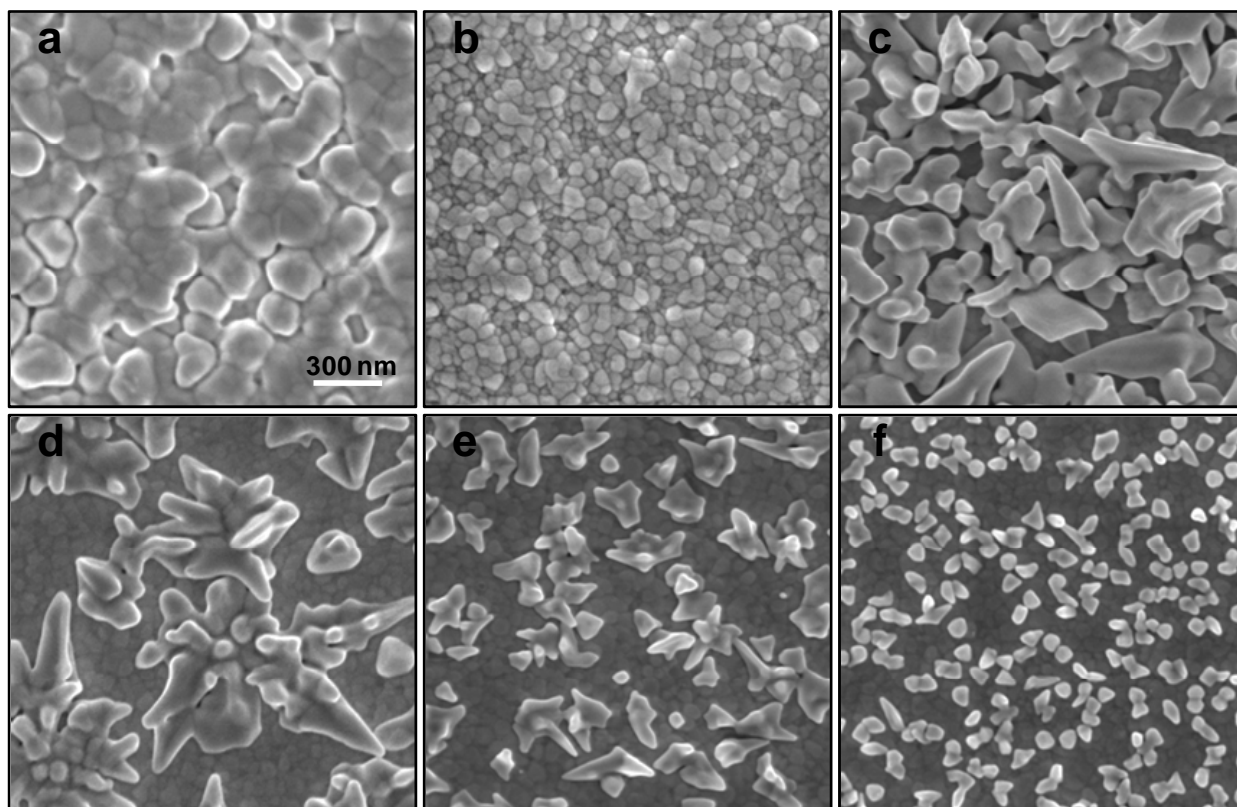


**Fig. S2** FESEM images (a-f) of BANCs (6 h growth) on Au-coated silicon wafer with respect to different conc. of HAuCl<sub>4</sub> (10, 5, 2, 1, 0.5, and 0.05 mM). The conc. of CTAB and AA is 16 mM and 4 mM respectively.

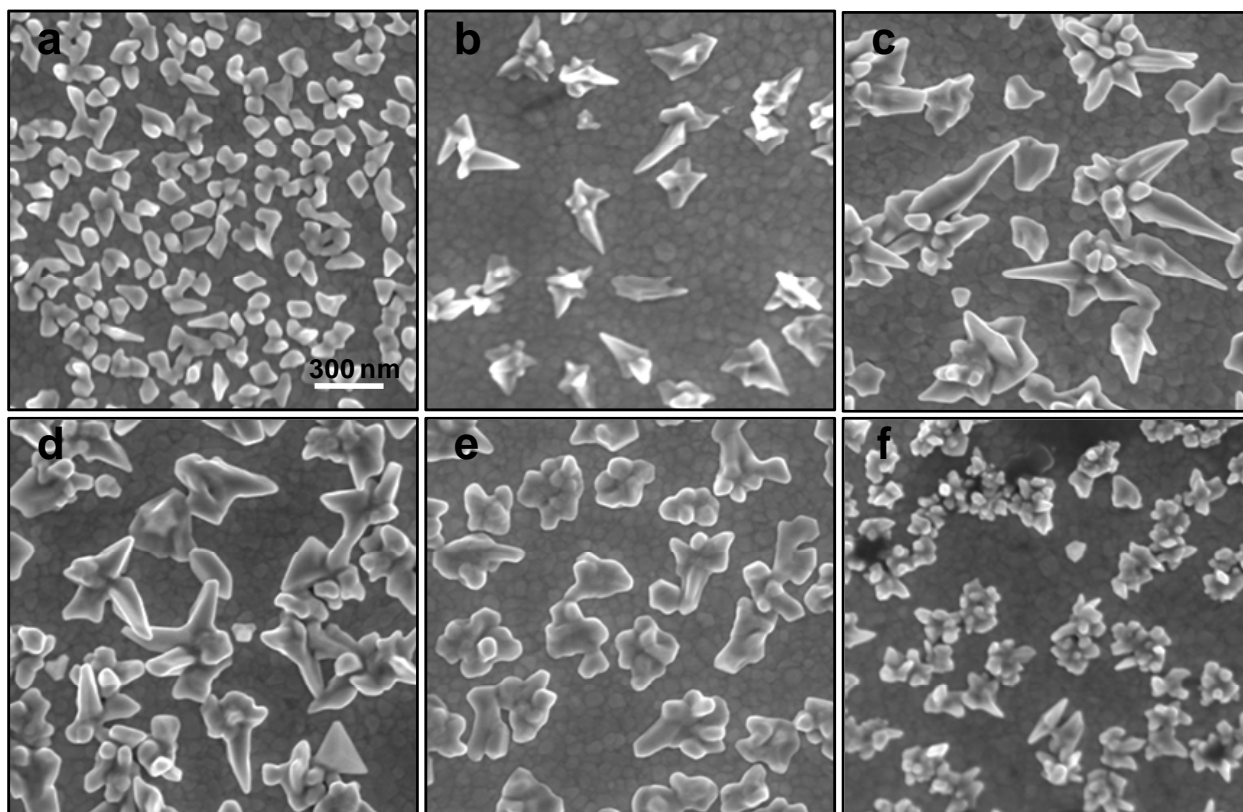


**Fig. S3** FESEM images (a-f) of BANCs (6 h growth) on Au-coated silicon wafer with respect to different conc. of AA (40, 16, 8, 4, 2, and 0.2 mM). The conc. of CTAB and AA is 16 mM and 1 mM respectively.



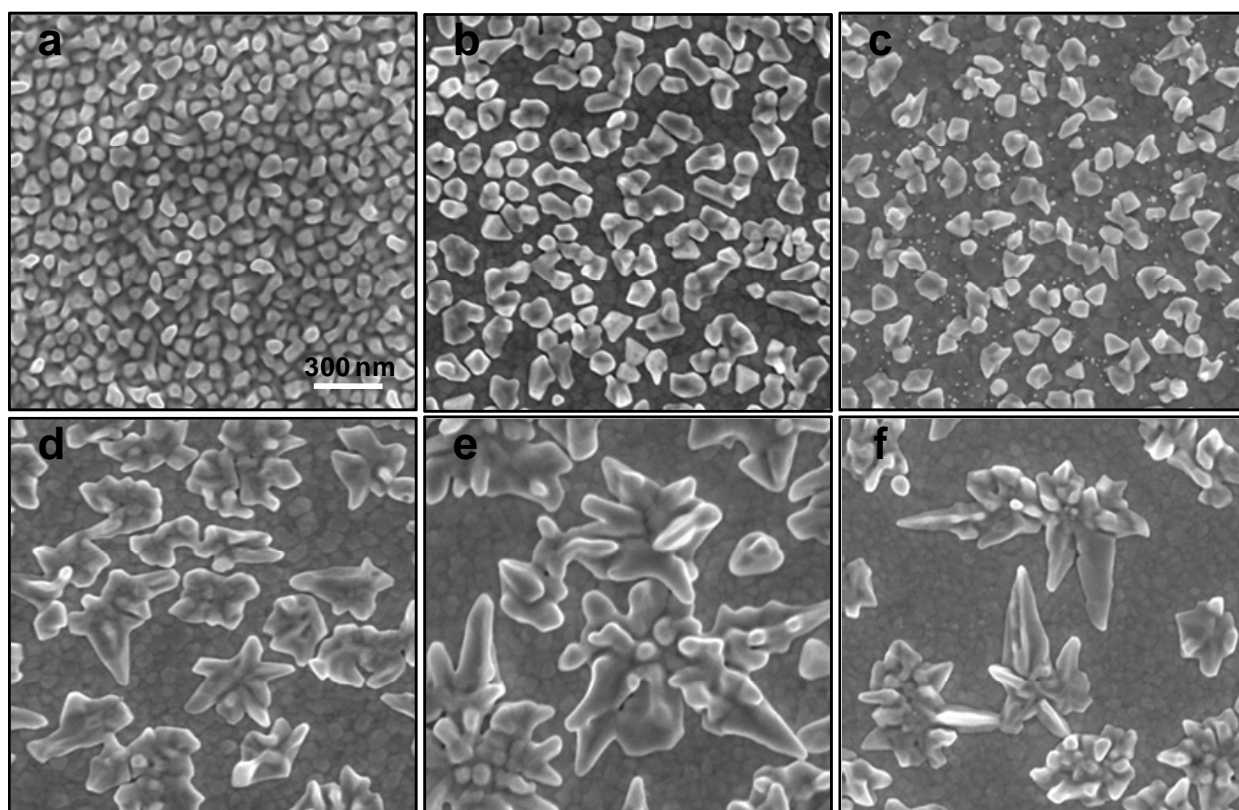


**Fig. S4** FESEM images (a-f) of BANCs (6 h growth) on Au-coated silicon wafers modified with different conc. of HDT SAM (0, 0.01, 0.1, 1, 15, and 20 mM). The conc. of CTAB, HAuCl<sub>4</sub> and AA is 16, 1 and 4 mM respectively.

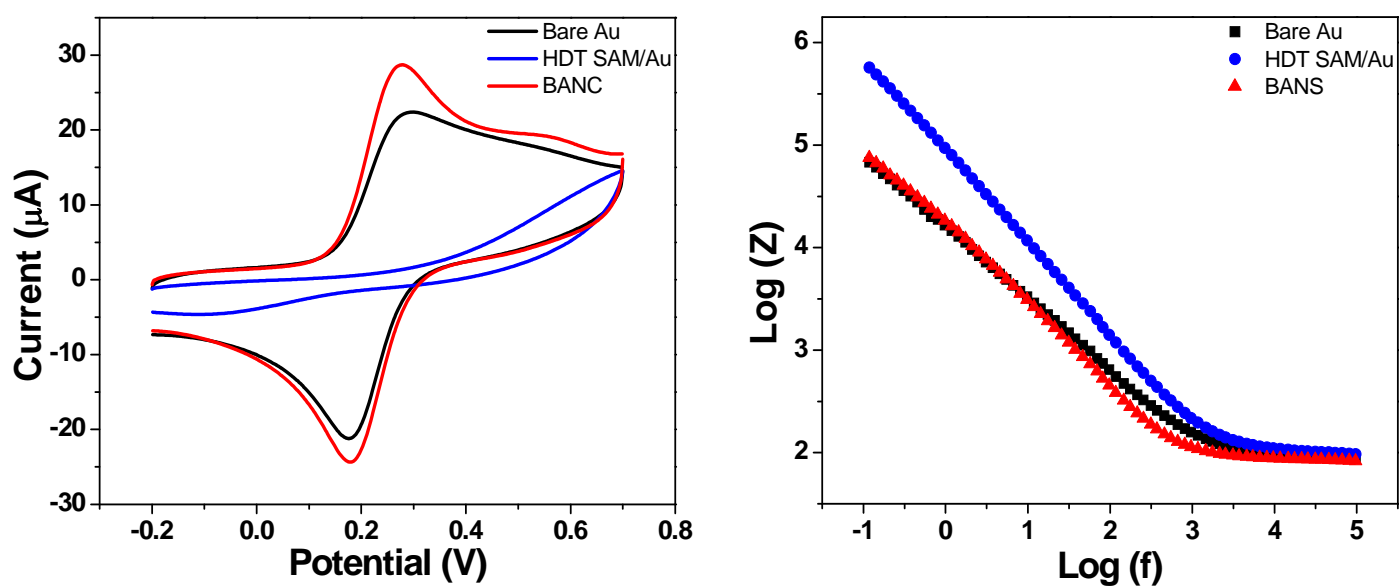


**Fig. S5** (a) Cyclic voltammetric and impedance (b) responses of bare Au (black line), HDT SAM (blue line) and BANCs (red line) modified electrodes in 1 mM  $\text{Fe}(\text{CN})_6^{4-/3-}$  containing 0.1 M PBS. The scan rate is  $100 \text{ mVs}^{-1}$ .



**Table S1**

Table containing the assignment of different SERS bands of UA.<sup>a</sup>

| Raman Shift (cm <sup>-1</sup> ) | Band Assignment                          |
|---------------------------------|--|
| 507                             | $\delta(\text{C}_8=\text{O})$            |
| 639                             | $\delta$ (ring)                          |
| 998                             | C-N <sub>7</sub>                         |
| 1301                            | $\nu(\text{C}_2\text{-N}) + \text{ring}$ |
| 1438                            | N <sub>1</sub> -H                        |
| 1488                            | N <sub>3</sub> -H                        |
| 1592                            | $\nu(\text{C}=\text{C}) + \text{ring}$   |

a- based on reference: Majoube, M.; Vergoten, G. *J. Mol. Struct.* 1993,**294**, 41-44.

$\nu$  : stretch;  $\delta$  : in plane bend